J Therm Anal Calorim (2017) 128:125–134
DOI 10.1007/s10973-016-5884-x

Analysis on oxidation process of sulfurized rust in oil tank

Z. Dou[1] · J. C. Jiang[1] · S. P. Zhao[1] · W. X. Zhang[1] · L. Ni[1] · M. G. Zhang[1] · Z. R. Wang[1]

Received: 13 February 2016 / Accepted: 1 October 2016 / Published online: 16 November 2016

Abstract The paper focuses on the oxidation process of sulfurized rust in crude oil tank. Firstly, one sort of rust was put into the sulfurization and oxidation experimental apparatus. The chemical compositions and phase of sulfurized rust were analyzed by energy-dispersive X-ray spectrometer–scanning electron microscope technique. The result shows that the main contents are S, Fe and O and give a short length of side and diamond appearance, and a large pore size in structure. The oxidation of sulfurized rust at ambient temperature was investigated, which transferred from electrochemical reactions to chemical reactions. The result of thermal decomposition experiment indicates that the product of electrochemical reactions is ferrous sulfate. Hereafter, the thermo-gravimetric/differential scanning calorimetric (TG/DSC) technique was used to evaluate the self-heating hazards of pre-oxygenized sulfurized rust. The given TG/DSC curves at different heating rates are similar. Every curve consisted of three weightlessness stages and two weight gain stages. The corresponding apparent activation energy values, most probable kinetic model functions and pre-exponential factor values were calculated by the Flynn–Wall–Ozawa method, the Achar–Brindley–Sharp–Wendworth method and the Kissinger method. The final results described the complexity of oxidation process of pre-oxygenized sulfurized rust.

✉ J. C. Jiang
jcjiang@njtech.edu.cn

✉ Z. R. Wang
wangzr@njtech.edu.cn

[1] Jiangsu Key Laboratory of Hazardous Chemicals Safety and Control, Jiangsu Key Laboratory of Urban and Industrial Safety, College of Safety Science and Engineering, Nanjing Tech University, Nanjing 210009, China

Keywords Oil tank · Sulfurized rust · Oxidation self-heating · Kinetic mechanism

Introduction

As it is known, rust formed on the inside walls and respiratory/safety valve inner cavity of tanks and pipelines reacts with hydrogen sulfide at low-temperature, which results in the formation of sulfurized rust in the process of transportation and storage of crude oil and natural gas [1–6]. In general, the principal iron sulfides of sulfurized rust are FeS and Fe_3S_4 at normal temperature, and the components of sulfurized rust are changed along with the rising in temperature. The higher temperature leads the transformation from FeS to Fe_3S_4 and FeS_2 [7–9]. Temperature rise brings about iron sulfides along the route

$$FeS \rightarrow Fe_3S_4 \rightarrow FeS_2 \quad (1)$$

Possible reactions are

$$3FeS + S \rightarrow Fe_3S_4 \quad (2)$$

$$Fe_3S_4 + 2S \rightarrow 3FeS_2 \quad (3)$$

Once exposed to the air, the sulfurized rust can lead to a mass of heat release. If the generation of heat is faster than the release, it may result in accumulating of the heat and rising its temperature, finally fire and explosion accident because of this sulfurized rust being an ignition resource [8–10]. Some fire and explosion accidents have been reported in the literature [6, 11]. The self-heating process of sulfurized rust in the atmosphere has been studied in detail. It is thought that the sulfurized rust which includes mackinawite (FeS), greigite (Fe_3S_4) and pyrite (FeS_2) could react with oxygen as following [4, 5, 7, 8, 12]:

$$4FeS + 7O_2 = 2Fe_2O_3 + 4SO_2,\ \Delta H = -805\,\mathrm{kJ\,mol^{-1}} \quad (4)$$

$$4Fe_3S_4 + 25O_2 = 6Fe_2O_3 + 16SO_2,\ \Delta H = -2100\,\mathrm{kJ\,mol^{-1}} \quad (5)$$

$$4FeS_2 + 11O_2 = 2Fe_2O_3 + 8SO_2,\ \Delta H = -827\,\mathrm{kJ\,mol^{-1}} \quad (6)$$

However, the oxidation process of sulfurized rust is very complicated, and it could not be easily described as the three equations at above. Besides, the literatures dealing with thermal analysis for oxidation of sulfurized rust are devoid. Dou [13] had made use of the Madhusudanan–Krishnan–Ninan method and the master plot method to calculate the apparent activation energy values, most probable kinetic model functions and pre-exponential factor values, but the temperature-programmed methods have not been applied to study the details of oxidation process of sulfurized rust widely. The temperature-programmed methods consist of differential scanning calorimetric (DSC), TG and differential thermal analysis (DTA) [14–16].

In this research, the chemical compositions of sulfurized rust are analyzed by precision instrument. The self-heating process of sulfurized rust is studied at first, and combining with the TG/DSC–FTIR (Fourier Transform Infrared Spectroscopy) results the deeper analysis is developed. After that, the apparent activation energies, the most probable kinetic model functions and the pre-exponential factors for the different stages of oxidation process are determined on the basis of TG results with the usage of integral and differential methods.

Experimental

Sulfurized rust preparation

The rust sample was collected from respiratory valve inner cavity of a crude oil tank in Jinling Petrochemical Company, and its major ingredient was rust. The particle diameter of the sample was ground to less than 250 μm and dried at 120 °C for 6 h in an oven to remove water.

Before oxidation experiment, 10 g of rust sample was sulfurized in the sulfurization and oxidation experimental apparatus. The sulfurization and oxidation experimental apparatus had the following four parts. Part 1 was the gas supply section, which included air cylinder, nitrogen cylinder, hydrogen sulfide cylinder and gas buffering and flow rate control. Part 2 was the airflow rate and humidification measurement section, which contained a cone bottle with water and flow meter. Part 3 was the sulfurization and oxidation section, which involved a quartz tube twined with an electric heating tape and thermocouple. Part 4 was the tail gas monitoring, buffering and absorption section, which was comprised of a SO_2 concentration meter, an empty cone bottle and a conical flask with sodium hydroxide solution. Figure 1 shows the sulfurization and oxidation experimental apparatus.

Prior to the sulfurization, the 10 g sample was placed in quartz tube that was fitted with glass wool plugs and taps at both ends. Then the gas route was connected and gas tightness of apparatus was checked. The air in apparatus was replaced by high purity nitrogen from N_2 cylinder with only valves V2, V4, V7, V9 open. The electric heating tape was wrapped around the quartz tube to keep the sample at 35 °C because of the operating temperature of crude oil tank ranging from 25 to 35 °C. Afterward, the sulfurization gas (made up of H_2S and N_2, V_{H2S}:V_{N2} = 2:3) passed through the water at the rate of 500 mL min^{-1} with valves V2, V3, V4, V5, V6, V9 open and other valves closed. This could make sure that the gas would be saturated with water in a similar condition as found in the crude oil tank. As none of the other gases was produced in this process, the remainder of hydrogen sulfide was absorbed by NaOH solution. After 6-h sulfurization, the sulfurized rust was cooled till its temperature reached the ambient temperature. In order to increase the accuracy of experiments, the sulfurization of rust was repeated three times.

Oxidation of sulfurized rust in the atmosphere

After sulfurized rust preparation, two 10 g samples were used for the oxidation experiment. Before oxidation, the apparatus was filled with high purity nitrogen from N_2 cylinder with only valves V2, V4, V7, V9 open for 15 min till all the hydrogen sulfide had been exhausted. As one sample reacting with wet air-like environmental conditions in the field, the valves V1, V4, V5, V6, V8, V10 were open and other valves closed. The other sulfurized sample was dried at 80 °C for 60 min firstly with only valves V2, V4, V7 open; meanwhile, N_2 was passed through the quartz tube at the rate of 500 mL min^{-1}; then, the dry sulfurized rust was cooled down to room temperature. Subsequently, the dry air flowed through the dry sulfurized rust with V1, V4, V7, V8, V10 open and other valves shut. In order to increase the accuracy of experiments, oxidation of the two sulfurized rust were repeated three times.

The chemical compositions analysis of sulfurized rust

The sulfurized rust obtained in sulfurization and oxidation experimental apparatus was analyzed by the application of energy-dispersive X-ray spectrometer (EDS)–scanning electron microscope (SEM) technique in detail. Surfaces of the randomized particles and the pressed disks of the sulfurized rust were scanned, and the element compositions

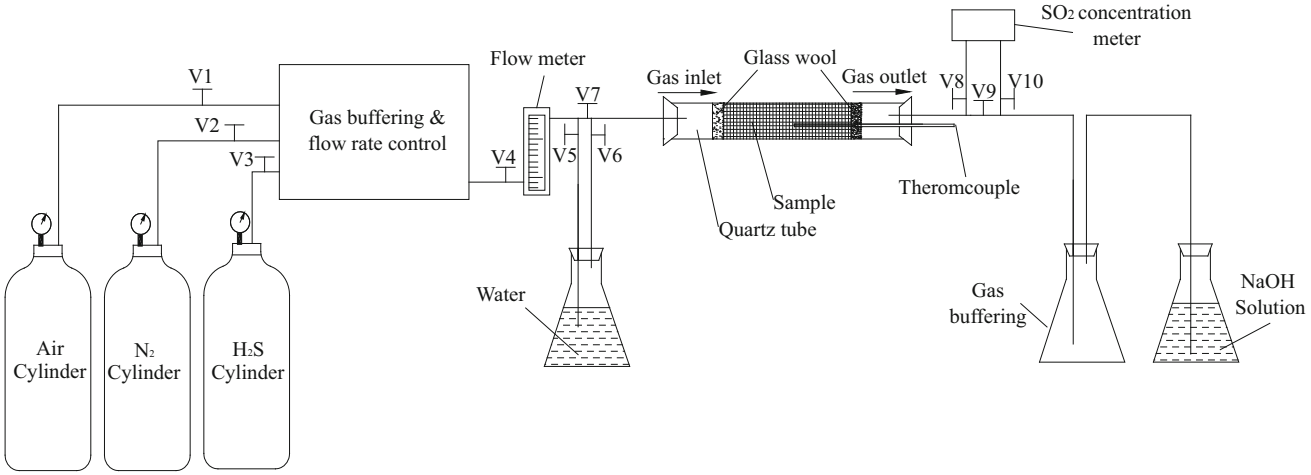

Fig. 1 Sulfurization and oxidation experimental apparatus

were determined with scanning electron microscope JEOL-JSM-5600 equipped with a dispersive X-ray spectrometer Noran Vantage DSI.

The energy-dispersive X-ray spectrometry analysis of sulfurized rust is presented in Fig. 2, and combining with the previous studies the corresponding possible chemical compositions are listed in Table 1. Figure 3 shows that the sulfurized rust gave a short length of side, diamond appearance and a large pore size in structure that enhanced the tendency of spontaneous combustion.

TG/DSC-FTIR test

Thermo-gravimetric (TG) and differential scanning calorimetry (DSC) are the most commonly used techniques in understanding the course of solid-state reactions. The relative sensitivity of TG/DSC depends on the change in mass or enthalpy of the process [14]. In this study, TA Instrument SDT-Q600 equipped with Nicolet 6700 FTIR Spectrometer of Thermo Scientific was used for thermal analysis at the temperature ranging from 30 to 900 °C in both nitrogen atmosphere and air corresponding to the sulfurized rust decomposition and oxidation; the N_2 and air were at flow rate of 100 mL min^{-1}. For both the thermal decomposition and the oxidation, the heating rates are 5, 10, 20 and 40 °C min^{-1}, respectively. The sample of sulfurized rust for each experiment was about 5 mg.

Results and discussion

The curves of temperature versus time (0–1000 s) for oxidation of sulfurized rust with moist air and dry air are presented in Fig. 4. It is evident that the water in the

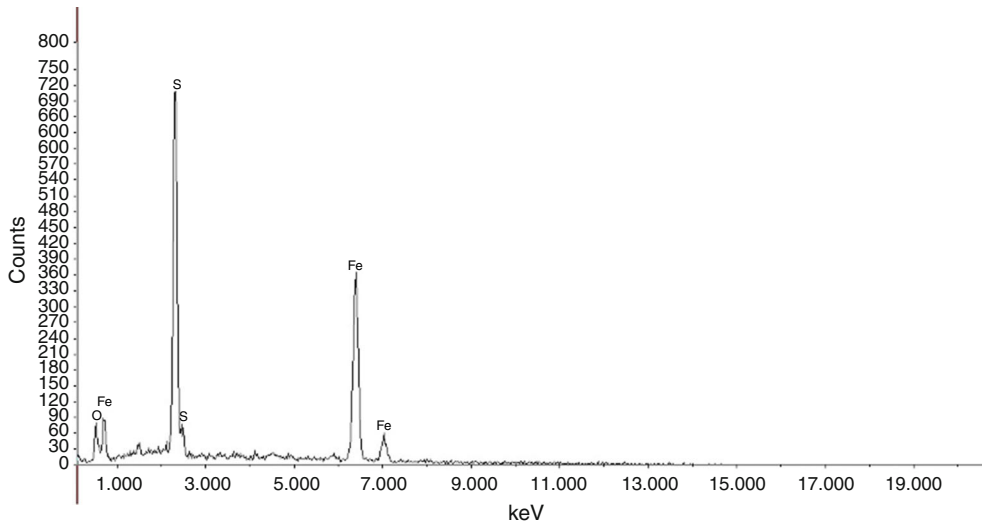

Fig. 2 EDS of dry sulfurized rust

Table 1 Chemical compositions of sulfurized rust

Samples	Elements	Mass fraction/%	Possible components
Wet sulfurized rust	Fe	78.75	S
	S	21.25	Fe_2O_3
	O	9.33	FeS
			Fe_3S_4
			FeS_2

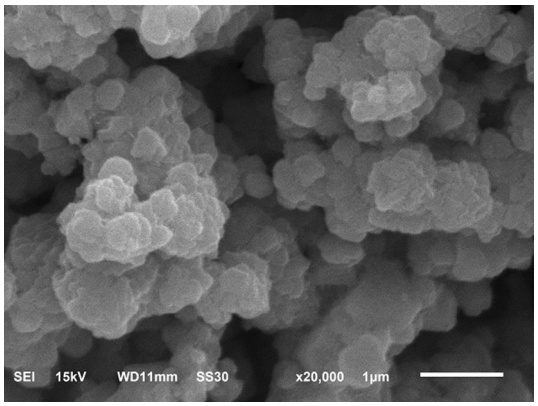

Fig. 3 SEM image of sulfurized rust

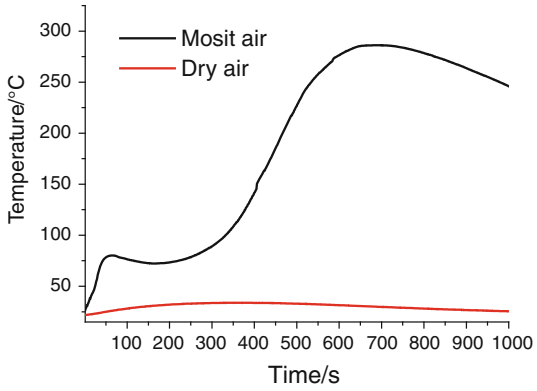

Fig. 4 Temperature versus time for oxidation of sulfurized rust with moist air and dry air

sulfurized rust and moist air accelerated the oxidation. The reaction of wet sulfurized rust with moist air was violent and rapid. As it is presented in Fig. 4, there were two rapid self-heating stages in the oxidation process of wet sulfurized rust with moist air, while dry sample reacted with dry air slowly. For the oxidation of wet sulfurized rust with moist air, the temperatures and times corresponding to the ends of different self-heating stages are listed in Table 2. And it also gives the peak temperature and the corresponding time of oxidation process of dry sulfurized sample with dry air.

In the oxidation experiment of wet sulfurized rust with moist air, the vitriol fog was observed in the gas buffering conical flask and a pungent odor identified to be SO_2 by pH indicator paper. Figure 5 presents the temperature and SO_2 concentration versus time for oxidation process of wet sulfurized rust with moist air. Because of the SO_2 concentration reaching the max value of scale range (4800 ppm), there is a flat in the curve of SO_2 concentration versus time.

According to Fig. 5, at the time of 83 s the double derivative in time t of temperature T equaled to zero and the SO_2 occurred at 85 s simultaneously. The time SO_2 occurring later 2 s may be as a result of the meter error and the time allowed SO_2 flowing from quartz tube to the meter. Considering the ending time of the first rapid self-heating stage, the time that the double derivative in time t of temperature T equaled to zero and the time SO_2 appearing, the other oxidation experiment was finished to figure the reactions in the first self-heating stage. Firstly, the wet sulfurized rust was oxygenized 80 s with moist air. Then the pre-oxygenized sulfurized rust was put in the SDT-Q600 for the thermal decomposition experiment at heating rate of 5, 10, 20 and 40 °C min^{-1} from 30 to 900 °C in nitrogen atmosphere. The N_2 was at flow rate of 100 mL min^{-1}. During the thermal decomposition of pre-oxygenized sulfurized rust, a gas product occurred in the thermal decomposition according to Fig. 6. An FTIR spectrum of the gas was measured at the wavenumbers of 1135.72, 1163.62, 1346.49 and 1374.39 cm^{-1} after 100, 50, 25 and 12.5 min, respectively. As it is known that the infrared characteristic absorbing peaks of SO_2 are in the range of 1401–1304, 1229–1071 and 2523–2461 cm^{-1} [17], inhere the gas product was determined to be SO_2. The temperature of thermal decomposition had been about 500 °C since the wet sulfurized rust oxidation product was heated, and it is the common knowledge that iron sulfate starts decomposing at about 500 °C [18], from which it could be inferred that one or some sulfates occurred because of water existing in the wet sulfurized rust and the moist air. As referred above, oxidation of dry sulfurized rust with dry air was that slow and nothingness. Therefore, the first rapid self-heating stage referred in Fig. 4 is electrochemical oxidation reaction process, possible reactions are [19]

$$FeS = Fe^{3+} + S^0 + 3e \quad (7)$$

$$2FeS + 8H_2O = 2Fe^{3+} + 2SO_4^{2-} + 16H^+ + 18e \quad (8)$$

$$FeS_2 = Fe^{3+} + 2S^0 + 3e \quad (9)$$

$$FeS + 8H_2O = Fe^{3+} + 2SO_4^{2-} + 16H^+ + 15e \quad (10)$$

Table 2 Temperatures and the corresponding times of different stages during the oxidation of sulfurized rust

Sulfurized rust	Air	Temperature at the end of first rapid self-heating stage/°C	Time at the end of first rapid self-heating stage/s	Peak temperature/°C	Time corresponding to the peak temperature/s
Wet	Moist	80.06	61	286.2	685
Dry	Dry	None	None	33.88	336

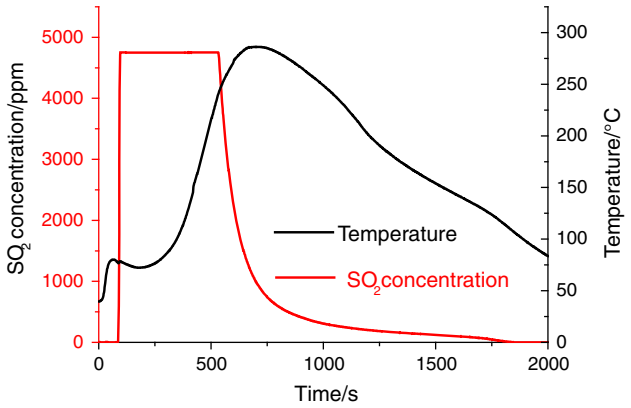

Fig. 5 Temperature and SO_2 concentration versus time for oxidation of wet sulfurized rust with moist air

$$O_2 + 4H^+ + 4e = 2H_2O \quad (11)$$

$$Fe^{3+} + e = Fe^{2+} \quad (12)$$

Besides, four 10 g pre-oxygenized sulfurized rust samples were prepared for thermal oxidation experiments ranging from 30 to 900 °C at heating rate of 5, 10, 20 and 40 °C min^{-1}, respectively, in air atmosphere. The curves of simultaneous TG–DTG–DSC analysis for the oxidation process of pre-oxygenized sulfurized rust in air at different heating rates are exemplarily shown in Figs. 7 and 8, which indicated the complexity of each oxidation process. At diverse heating rates, the gained curves for oxidation process of sulfurized rust samples were similar but with a little difference. In general, increase in the heating rates results in higher temperature values for the oxidation process. According to Fig. 7, all the oxidation processes at different heating rates could be broken up into five stages including three weightlessness stages and two weight gain stages. The obviously corresponding peaks could be found from TG curves, which showed the oxidation of the pre-oxygenized sulfurized rust, the formation and the decomposition of sulfates.

Table 3 gives the mass loss and gain and corresponding temperatures detected during the TG/DSC experiment at various heating rates. In the two weight gain stages, it could be thought that the generation of ferrous sulfate was the major chemical reaction for the former and the ferric sulfate was for the latter. At about 500 °C, dissociation of ferric sulfate starts, which is deduced from the weightlessness on the TG curves. A summary of oxidation reactions is written as follows [13, 19]:

$$S^0 + O_2 = SO_2 \quad (13)$$

$$4FeS + 7O_2 = 2Fe_2O_3 + 4SO_2 \quad (14)$$

$$S^0 + FeS = FeS_2 \quad (15)$$

$$4FeS_2 + 11O_2 = 2Fe_2O_3 + 8SO_2 \quad (16)$$

$$FeS_2 + 2O_2 = FeSO_4 + S^0 \quad (17)$$

$$2FeSO_4 + O_2 + SO_2 = Fe_2(SO_4)_3 \quad (18)$$

$$2Fe_2(SO_4)_3 = 2Fe_2O_3 + 6SO_2 + 3O_2 \quad (19)$$

The methods used for analysis of the data obtained from temperature-programmed experiments could be classified as differential and integral methods, and the two methods are sorted further on the basis of the data acquired from one or more heating rates [14]. It is generally acknowledged that methods in accordance with different heating rates lead to more infallible results than those based on a single heating rate.

In this study, both the differential method (Flynn–Wall–Ozawa method, FWO) and the integral method (Achar–Brindley–Sharp–Wendworth method, ABSW) had been used for calculating the apparent activation energies, the most probable kinetic model functions and the pre-exponential factors corresponding to the five weightlessness or weight gain stages. Moreover, the model-free method (Kissinger method) was applied to ensure the apparent activation energies and the pre-exponential factors more accurately. Flynn–Wall–Ozawa method [15, 20, 21] was used to quantify the dependence between the temperature and the heating in the following equation:

$$\lg \beta = \lg\left(\frac{AE}{RG(\alpha)}\right) - 2.315 - 0.4567\frac{E}{RT} \quad (20)$$

where β is heating rate; α is conversion ratio; A is the pre-exponential factor; E is the apparent activation energy, J; R is the gas constant, 8.314 J $mol^{-1}K^{-1}$; $G(\alpha)$ is the integral form of kinetic model function; T is temperature, K. For the Achar–Brindley–Sharp–Wendworth method [22–24], the equation is:

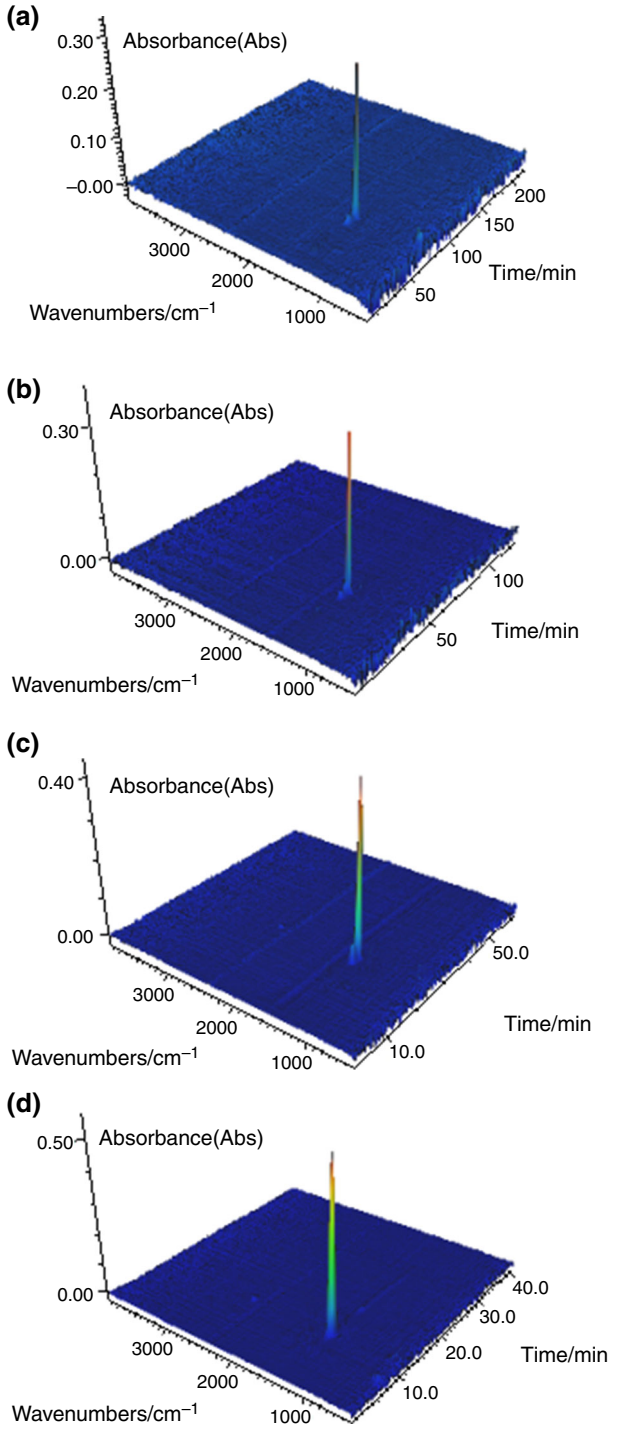

Fig. 6 Infrared spectrogram of decomposition of pre-oxygenized sulfurized rust at heating rate of **a** 5 °C min^{-1}, **b** 10 °C min^{-1}, **c** 20 °C min^{-1}, **d** 40 °C min^{-1}

$$\ln\left[\frac{\mathrm{d}\alpha}{f(\alpha)\mathrm{d}T}\right] = \ln\frac{A}{\beta} - \frac{E}{RT} \tag{21}$$

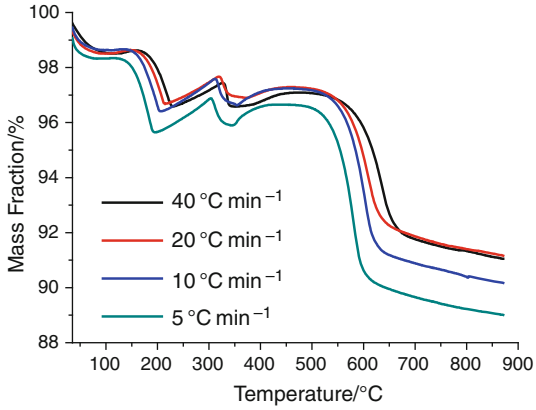

Fig. 7 TG curves of pre-oxygenized sulfurized rust at different heating rates

where $f(\alpha)$ is the differential form of kinetic model function. And the equation for the Kissinger method follows [25–28]:

$$\ln\left(\frac{\beta}{T_\mathrm{p}^2}\right) = \ln\frac{AR}{E} - \frac{E}{RT} \tag{22}$$

where T_p is the peak temperature. Both $G(\alpha)$ and $f(\alpha)$ utilized in the calculation of the apparent activation energies and the pre-exponential factors have 41 types of kinetic model function and one-to-one correspondence [29].

In order to determine the kinetic model parameters of thermal oxidation processes of sulfurized rust, the curves of conversion ratio verse reciprocal of temperature at different heating rates in five weightlessness or weight gain stages are presented in Fig. 9.

According to Fig. 9 and Eqs. (20), (21) and (22), the apparent activation energies and the pre-exponential factors for the diverse stages could be figured out with the knowledge of $G(\alpha)$, $f(\alpha)$, $1/T$, T_p, $\mathrm{d}\alpha/\mathrm{d}T$ and β. In principle, the kinetic model function would be ensured in conditions of (a) the E and lg$A$ values arranging from 80 to 250 kJ mol^{-1} and from 7 to 30 s^{-1}, respectively; (b) the E and IgA values separately obtained from FWO method and ABSW method being approximate; (c) good correlation, linear correlation coefficient $R^2 > 0.98$, standard deviation SD < 0.3; (d) the determined E and A from differential and integral methods being close to the values calculated from Kissinger method. Table 4 gives all apparent activation energies and the pre-exponential factors for the different weightlessness and weight gain stages which were computed from TWO, ABSW and Kissinger. The most probable kinetic model functions corresponding

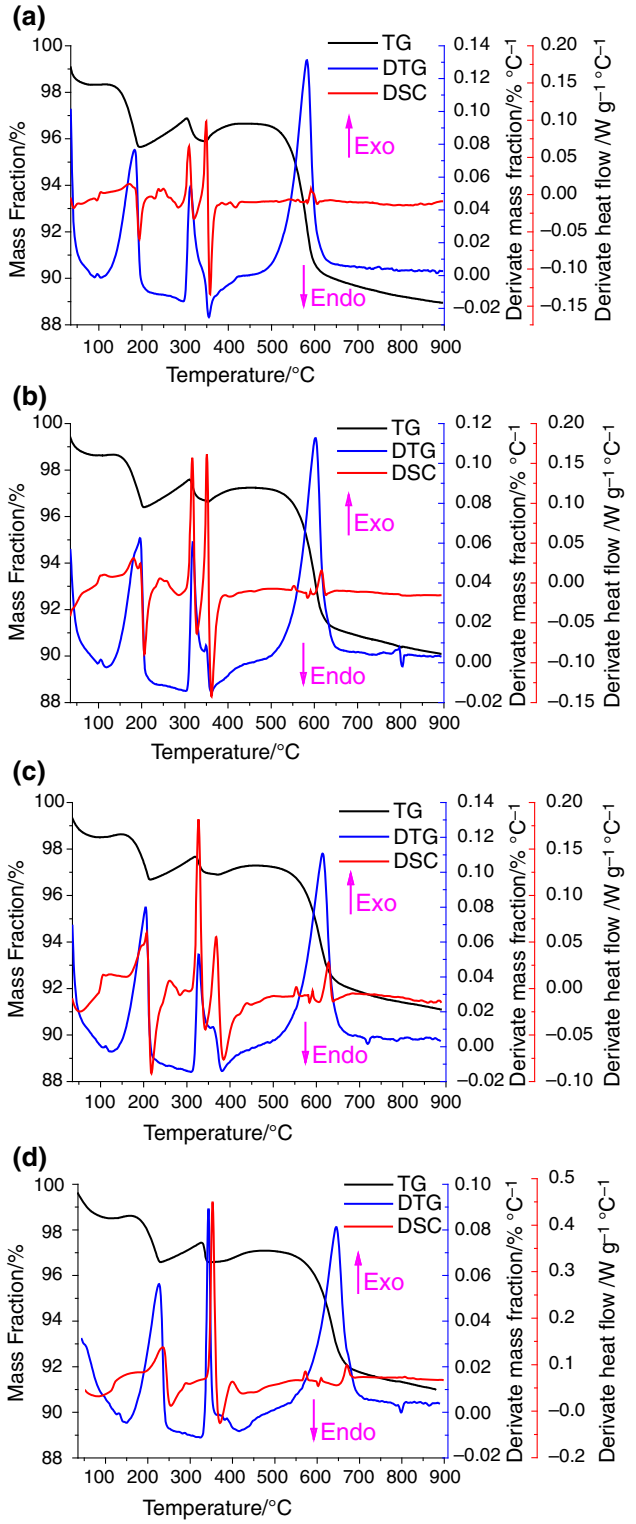

Fig. 8 TG–DTG–DSC curves of oxidation of pre-oxygenized sulfurized rust at heating rate of **a** 5 °C min^{-1}, **b** 10 °C min^{-1}, **c** 20 °C min^{-1}, **d** 40 °C min^{-1}

Table 3 Mass loss and gain and corresponding temperatures of TG curves

Heating rate (β)/°C min^{-1}	5	10	20	40
1st mass loss stage				
Initial temperature (T_{min})/°C	105	139	148	163
Initial mass (W_{max})/%	98.33	98.66	98.64	98.61
Final temperature (T_{max})/°C	194	204	214	228
Final mass (W_{min})/%	95.65	96.41	96.69	96.6
1st mass gain stage				
Initial temperature (T_{min})/°C	198	208	216	233
Initial mass (W_{max})/%	95.65	96.41	96.69	96.6
Final temperature (T_{max})/°C	303	309	317	324
Final mass (W_{min})/%	96.88	97.58	97.66	97.43
2nd mass loss stage				
Initial temperature (T_{min})/°C	305	312	321	329
Initial mass (W_{max})/%	96.88	97.58	97.66	97.42
Final temperature (T_{max})/°C	326	331	338	341
Final mass (W_{min})/%	96.03	96.81	97.04	96.61
2nd mass loss stage				
Initial temperature (T_{min})/°C	346	354	375	382
Initial mass (W_{max})/%	95.9	96.63	96.91	96.65
Final temperature (T_{max})/°C	422	442	451	463
Final mass (W_{min})/%	96.65	97.24	97.28	97.08
3rd mass loss stage				
Initial temperature (T_{min})/°C	495	491	506	521
Initial mass (W_{max})/%	96.56	97.2	97.21	97.01
Final temperature (T_{max})/°C	650	659	669	694
Final mass (W_{min})/%	89.95	91.11	92.07	91.8

to different weightlessness and weight gain stages are presented in Table 5.

On the basis of the study for the oxidation self-heating process and the mechanism of sulfurized rust, the understanding of sulfurized rust oxidizing progress in the wild is extended. In the initial stage of oxidation, electrochemical reactions occur with the generation of ferrous sulfate; however, as a result of reduction in water fraction in sulfurized rust the reaction rate decreases gradually till disappearance of water exists with no electrochemical reactions any more. Meanwhile, a part of reaction exothermal heat is absorbed by the sulfurized rust itself along with chemical reactions arising, the oxidation of sulfurized rust falls into the violent stage. According to the results of this research, the stagnation temperature range at which electrochemical reactions transfer to chemical reactions could be ascertained and develop a new monitoring and early warning method for operators in the field. Besides, the valid service life and the

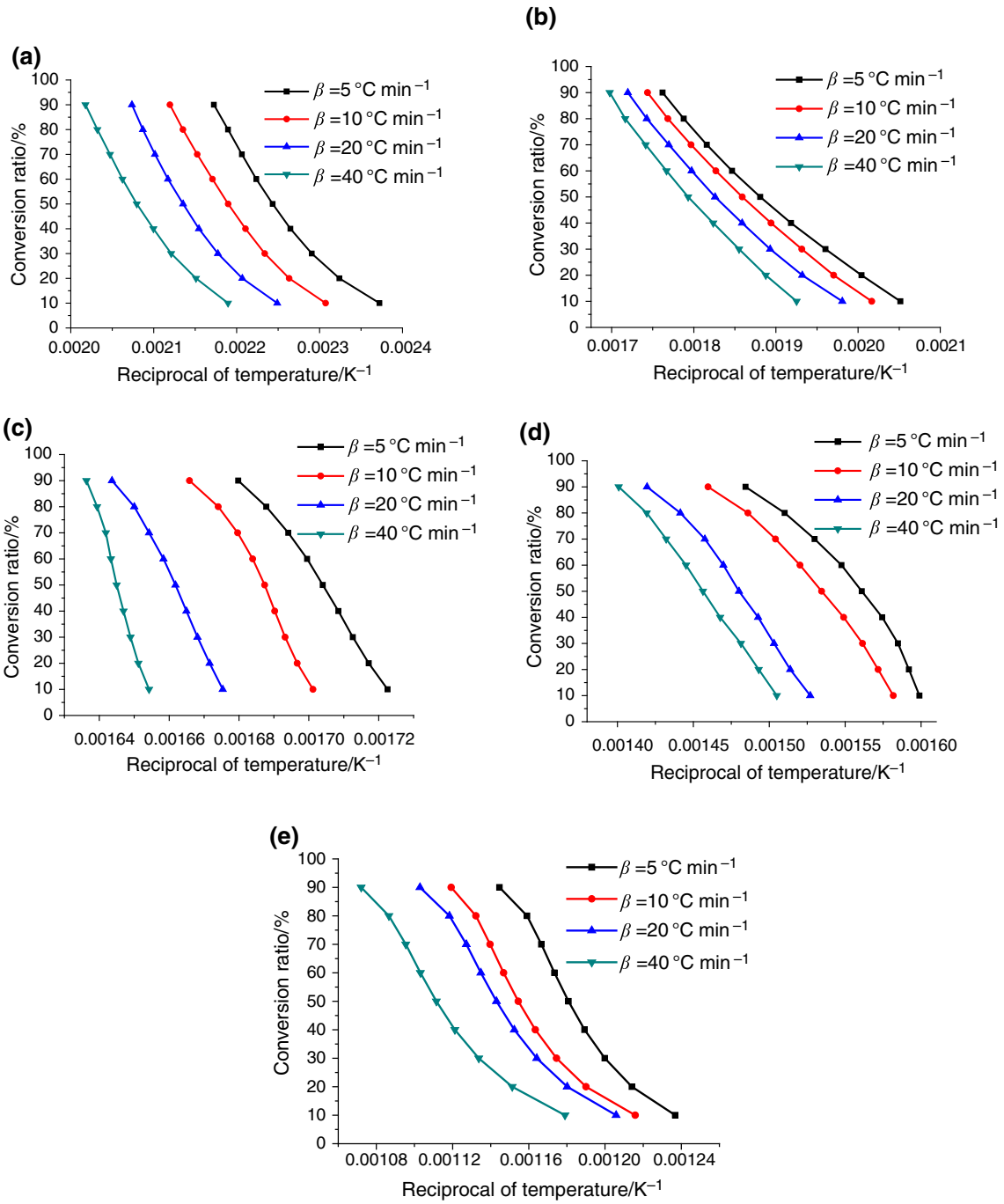

Fig. 9 Curves of conversion ratio verse reciprocal of temperature at different heating rates in the **a** 1st weightlessness stage of TG, **b** 1st weight gain stage of TG, **c** 2nd weightlessness stage of TG, **d** 2nd weight gain stage of TG, **e** 3rd weightlessness stage of TG

Table 4 Apparent activation energy and pre-exponential factor for the different weightlessness and weight gain stages

Stage	Apparent activation energy/kJ mol^{-1}			Denary logarithm pre-exponential factor/s^{-1}		
1st weightlessness stage	105.1	102.7	105.3	11.65	11.36	11.53
1st weight gain stage	251.9	245.7	285.2	24.02	23.41	25.92
2nd weightlessness stage	259.9	240.8	261.7	22.00	20.67	23.04
2nd weight gain stage	141.6	134.4	122.6	9.40	9.12	9.56
3rd weightlessness stage	239.7	258.5	240.1	13.97	15.08	13.95
Method	FWO	ABSW	Kissinger	FWO	ABSW	Kissinger

Table 5 $G(\alpha)$ and $f(\alpha)$ for the different weightlessness and weight gain stages

Stage	G(α)	$f(\alpha)$
1st weightlessness stage	$3[1-(1-\alpha)^{\frac{1}{3}}]$	$(1-\alpha)^{\frac{2}{3}}$
1st weight gain stage	$[-\ln(1-\alpha)]^3$	$\frac{1}{3}(1-\alpha)[-\ln(1-\alpha)]^{-2}$
2nd weightlessness stage	$1-(1-\alpha)^{\frac{1}{4}}$	$4(1-\alpha)^{\frac{3}{4}}$
2nd weight gain stage	$1-\frac{2}{3}\alpha-(1-\alpha)^{\frac{2}{3}}$	$\frac{3}{2}[(1-\alpha)^{-\frac{1}{3}}-1]^{-1}$
3rd weightlessness stage	$-\ln(1-\alpha)$	$1-\alpha$

optimum operating conditions of tank can be projected, which is an inherent safety measurement to avoid the emergence of fire and explosion.

Conclusions

For ascertaining the oxidation process of sulfurized rust produced in crude oil storage tank, fundamental research and experiments have been done.

The chemical compositions and phases of sulfurized rust are proved to be intricate by EDS and SEM. The main contents in sulfurized rust are S, Fe and O. The sulfurized rust gives a short length of side, diamond appearance and a large pore size in structure.

The oxidation of sulfurized rust with moist air is a complex process consisting of electrochemical reaction at first and then chemical reactions. In the initial stage, ferrous sulfate generated which could be demonstrated by the occurrence of SO_2 at about 500 °C in the thermal decomposition experiment of pre-oxidized sulfurized rust.

The TG/DSC curves for the pre-oxidized oxidation reaction of sulfurized rust in air at different heating rates are similar. Every curve could be divided into three weightlessness stages and two weight gain stages. For the weightlessness stage, the apparent activation energies for the 1st to the 3rd are in 102.7–105.3, 240.8–261.7 and 239.7–258.5 kJ mol^{-1}, respectively, the corresponding most probable kinetic model functions are $G(\alpha) = 3[1-(1-\alpha)^{\frac{1}{3}}]$, $G(\alpha) = 1-(1-\alpha)^{\frac{1}{4}}$ and $G(\alpha)=-\ln(1-\alpha)$, and the pre-exponential factor lg$A$ are among 11.36–11.65, 20.67–23.04 and 13.95–15.08 s^{-1} separately. For the 1st weight gain stage, the apparent activation energy is in 245.7–285.2 kJ mol^{-1}, the most probable kinetic model function is $G(\alpha)=[-\ln(1-\alpha)]^3$ and the pre-exponential factor lg$A$ is among 11.36–11.65 s^{-1}. For the 2nd weight gain stage, the apparent activation energy is in 122.6–141.6 kJ mol^{-1}, the most probable kinetic model function is $G(\alpha)=1-\frac{2}{3}\alpha-(1-\alpha)^{\frac{2}{3}}$ and the pre-exponential factor lg$A$ is among 9.12–9.56 s^{-1}. The apparent activation energies of the 1st weightlessness stage and the 2nd weight gain stage are much lower than others which mean the oxidation in these two stages more easily.

Acknowledgements The authors are grateful for the support given by key project of National Natural Science Foundation of China Under Grant No. 21436006, National Natural Science Foundation of China Under Grant No. 51176070, PHC-CaiYuanpei ("*Havu-Risk: Chemical industrial plants and domino effect: hazards, vulnerability, risks and sustainability*" 32114TE, 2014-2016), the Priority Academic Program Development of Jiangsu Higher Education Institutions of China and the Graduate Education Innovation Project of Jiangsu Province Under Grant No. CXLX13_440.

References

1. Zheng S, Chen L, Chen C. Failure analysis of an A333Gr6 pipeline after exposure to a hydrogen sulfide environment. Eng Fail Anal. 2013;35:516–23.
2. Walker R. Instability of iron sulfides on recently excavated artifacts. Stud Conserv. 2001;46(2):141–52.
3. Walker R, Steele AD, Morgan TDB. The formation of pyrophoric iron sulphide from rust. Surf Coat Technol. 1987;31(2):183–97.
4. Li P, Wang S, Zhang Z. Study on the effect of water on the formation and pyrophoricity of ferrous sulfide. Pet Sci Technol. 2011;29(18):1922–31.
5. Li P, Li JD, Zhao SL. Prevention of spontaneous combustion of sulfur-containing oil tanks. Pet Sci Technol. 2006;24(9):1009–17.
6. Zhao S, Wang C, Li P, Ding D, Wan X. The influence of sulfurization of rust in oil tanks. Energy Sour Part A. 2007;29(12):1111–9.
7. Walker R, Steele AD, Morgan D. Deactivation of pyrophoric iron sulfides. Ind Eng Chem Res. 1997;36(9):3662–7.
8. Walker R, Steele AD, Morgan D. Pyrophoric nature of iron sulfides. Ind Eng Chem Res. 1996;35(5):1747–52.
9. Walker R, Steele AD, Morgan TDB. Pyrophoric oxidation of iron sulphide. Surf Coat Technol. 1988;34(2):163–75.
10. Hughes RI, Morgan TDB, Wilson RW. Is pyrophoric iron sulphide a possible source of ignition? Nature. 1974;248(5450):670.
11. Zhao SP, Jiang JC, Zheng J. Thermal analysis on kinetics of thermal decomposition of FeS. J Chongqing Univ. 2011;34(1):140–4.
12. Li P, Li JD, Zhao SL. Research on the danger of fires in oil tanks with sulfur. Fire Saf J. 2005;40(4):331–8.
13. Dou Z, Jiang JC, Wang Z. Kinetic analysis for spontaneous combustion of sulfurized rust in oil tanks. J Loss Prev Process Ind. 2014;32:387–92.
14. Hu RZ, Gao SL, Zhao FQ, Shi QZ, Zhang TL, Zhang JJ. Kinetics of thermal analysis. 2nd ed. Beijing: Science Publishing House; 2008 **(in Chinese)**.
15. Ozawa T. Thermal analysis-review and prospect. Thermochim Acta. 2000;355(1):35–42.
16. Wagner M. Application handbook thermal analysis: thermal analysis in practice. Schwerzenbach: Mettler Toled; 2009.
17. Wierzejewska-Hnat M, Schriver A, Schriver-Mazzuoli L. FT infrared study of sulfur dioxide dimer. I. Nitrogen matrix. Chem Phys. 1994;183:117–26.
18. Kolta GA, Aska MH. Thermal decomposition of some metal sulphates. Thermochim Acta. 1975;11:65–72.
19. Li ZJ. Investigation on the mechanism of spontaneous combustion of sulphide ores and the key technologies for preventing fire. Changsha: Central South University; 2007.

20. Zhu FL, Feng QQ, Xu YF, Liu RT, Li KJ. Kinetics of pyrolysis of ramie fabric wastes from thermogravimetric data. J Therm Anal Calorim. 2015;119(1):651–7.
21. Zhang CF, Liu XD, Cheng J, Zhang JY. Study on curing kinetics of diglycidyl 1,2-cyclohexane dicarboxylate epoxy/episulfide resin system with hexahydro-4-methylphthalic anhydride as a curing agent. J Therm Anal Calorim. 2015;120(3):1893–903.
22. Criado JM, Gonzalez F, Morales J. Application of programmed temperature decomposition to the study of solid decomposition reactions taking place through the prout and tompkins mechanism. Thermochim Acta. 1975;12:337–42.
23. Yan L, He B, Hao T. Thermogravimetric study on the pressurized hydropyrolysis kinetics of a lignite coal. Int J Hydrog Energy. 2014;39(15):7826–33.
24. Xu Y, Zhang YF, Zhang GJ, Guo YF, Zhang J, Li GQ. Pyrolysis characteristics and kinetics of two Chinese low-rank coals. J Therm Anal Calorim. 2015;122(2):975–84.
25. Farjas J, Roura P. Exact analytical solution for the Kissinger equation: determination of the peak temperature and general properties of thermally activated transformations. Thermochim Acta. 2014;598:51–8.
26. Bai Y, Yang P, Zhang S, Li YQ, Gu Y. Curing kinetics of phenolphthalein-aniline-based benzoxazine investigated by non-isothermal differential scanning calorimetry. J Therm Anal Calorim. 2015;120(3):1755–64.
27. Shi N, Dou Q. Non-isothermal cold crystallization kinetics of poly(lactic acid)/poly(butylene adipate-co-terephthalate)/treated calcium carbonate composites. J Therm Anal Calorim. 2015;119(1):635–42.
28. Tripathi M, Kumar D, Rajagopal C, Roy PK. Curing kinetics of self-healing epoxy thermosets. J Therm Anal Calorim. 2015;119(1):547–55.
29. Yi J, Zhao F, Wang B. Thermal behaviors, nonisothermal decomposition reaction kinetics, thermal safety and burning rates of BTATz-CMDB propellant. J Hazard Mater. 2010;181(1–3):432–9.